Hierarchical micro-/macroporous TS-1 zeolite epoxidation catalyst prepared by steam assisted crystallization

Valentin Smeets [a], Eric M. Gaigneaux [a], Damien P. Debecker [a,*]

[a] Institute of Condensed Matter and Nanosciences (IMCN), UCLouvain, Place Louis Pasteur, 1, Box L4.01.09, 1348 Louvain-la-Neuve, Belgium. * E-mail: damien.debecker@uclouvain.be

Abstract:

Mesoporous Ti–SiO_2 nanoparticles were prepared under alkaline conditions in the presence of a surfactant and were subsequently converted into a hierarchical micro-/macroporous TS-1 zeolite with large crystal size using steam assisted crystallization. In this procedure, the precursor nanoparticles were used both as macroporous hard template and as Si and Ti sources. The secondary macroporosity is a reminiscence of the nanoparticles which undergo dissolution and recrystallization upon steaming. The obtained catalyst has structural properties comparable to benchmark TS-1. We show that the successful conversion of the amorphous material into a fully crystalline catalyst stands for its excellent catalytic performance in aqueous media. Besides, the combination of large crystal size with a hierarchical pore structure ensures easy catalyst handling and processing without compromising on the catalytic activity.

Keywords: hierarchically porous zeolite, TS-1, macroporous material, steam assisted crystallization, epoxidation

1. Introduction

Titanium silicalite-1 (TS-1) zeolite [1] is an important functional material that has been used for the past decades as a selective oxidation catalyst, *e.g.* in olefin epoxidation [2]. While preserving the MFI type structure that ensures its remarkable activity, it is desirable to design new TS-1 based catalysts for specific catalytic applications and reactor configurations.

On the one hand, catalytic performance is strongly limited by the slow diffusion of reactants and products in the micropores of the zeolite [3–6]. In some cases, the molecules cannot enter the microporosity and are thus restrained to the external surface. Therefore, strategies are put in place to enhance the surface-to-volume ratio of the catalyst, *i.e.* to reduce the diffusion path length within the inorganic walls and/or to increase the external surface area [4]. Thus, TS-1 can be shaped [7] as nano-sheets [8], pillared materials [9], membranes [10], etc. Another way out is to add a secondary porosity [11–14], with benefits in terms of active site accessibility. This was previously reported for micro-/mesoporous TS-1 [15–17], but the strategy was also shown to be applicable to micro-/macroporous TS-1 [18] as well as three level micro-/meso-/macroporous structures [19–21] and hollow TS-1 crystals [22,23]. More simply, the crystals size can be reduced in order to increase the catalytic performance.

On the second hand, the handling of small zeolite nanocrystals is complicated because such colloidal objects are refractory to mechanical recovery by filtration or decantation. Zeolite nanocrystals cannot be implemented in fixed bed flow reactor as their packing would result in an excessive pressure drop. Therefore, another objective of the modification of TS-1 materials is to obtain larger objects which fully benefit from the advantages of heterogeneous catalysts in terms of recoverability and reusability. Thus, TS-1 material can be prepared in the form of hierarchically porous microparticles [24,25] or even self-standing monoliths [26]. Alternatively, the nanosized crystals can be dispersed onto a porous support, *e.g.* diatomites [27].

Considering the above, it is highly desirable to obtain large crystals while preserving a high surface-to-volume ratio. The *Steam Assisted Crystallisation* (SAC) method, also called *Dry Gel Conversion* (DGC), has become a popular procedure to prepare hierarchically porous zeolites with a good control on texture and particle size [28–32]. In this method, an amorphous (mixed) oxide is prepared in the form of a dry gel and treated under hydrothermal conditions in the presence of a structure-directing agent and of steam. Upon steaming, the crystallization of the zeolite proceeds via an oriented attachment route, which consists in the aggregation and alignment of tiny crystallites that form bigger crystals [29]. This technique therefore differs from the hydrothermal synthesis of zeolites, the latter involving the crystallization route by nucleation and growth in liquid phase water. The particle size can be tuned by varying the temperature and crystallization time, whereas the porosity is typically controlled in the mesoporous range by the addition of templates – *e.g.* organosilanes – that prevent the fusion of the crystallites, or by leveraging on the grinding and drying steps of the gel prior to autoclaving [32]. Alternatively, Schwieger and co-workers showed that mesoporous silica and aluminosilicate nanoparticles could be used both as hard template and precursors in the synthesis of micro-/macroporous silicalite and ZSM-5 by SAC, respectively [33,34].

Herein, we propose to combine titanium and silicon precursors in the synthesis of amorphous Ti–SiO_2 nanoparticles and to use the latters in the preparation of hierarchical TS-1 material featuring both a micro-/macroporosity and large crystal size. To the best of our knowledge, the incorporation of titanium in such precursor material and its further crystallization into fully functional hierarchical TS-1 catalyst by SAC has never been reported. We aim to demonstrate that controlling the incorporation of titanium during the preparation of the precursor particles prior to the thermal treatment allows obtaining TS-1 presenting both proper Ti speciation in the MFI-type structure and a secondary intracrystalline macroporosity. The successful conversion of the amorphous material into crystalline TS-1 is exploited in the catalytic conversion of allyl alcohol into glycidol in water, and compared to the benchmark microporous TS-1 catalyst.

2. Experimental

2.1. Preparation of the materials

2.1.1. Preparation of the reference catalyst

Benchmark TS-1 ('**TS-1**') was prepared with a Ti loading of 1.8% (here and after the loading is expressed as mol Ti / (mol Ti + mol Si) × 100 %) using titanium isopropoxide (TiiP) and tetraethyl orthosilicate (TEOS) as Ti and Si sources, respectively, and tetrapropylammonium hydroxide (TPAOH) as structure directing agent [35]. The detailed preparation procedure is available in the Electronic Supplementary Information.

2.1.2. Preparation of the hierarchical micro-/macroporous TS-1

The micro-/macroporous TS-1 (denoted as '**TS-1_MAC**') was prepared by adapting the procedure of Machoke *et al.* for the preparation of macroporous silicalite [33]. First, mesoporous Ti–SiO_2 particles, denoted '**MSTP**', were synthesized as follows: 1 g of hexadecyltrimethylammonium bromide (CTAB, Alfa Aesar, 98%) was added to 140 ml distilled H_2O and 480 ml EtOH under stirring. After 10 min stirring, 24 ml NH_4OH 25% wt. aq. (Merck) was added (Solution A). In a separate vessel, 3.130 g TEOS and 0.097 g titanium butoxide (1.8% at. Ti) (TiBuO, Sigma-Aldrich, 97%) were mixed in 5 ml EtOH under vigorous stirring and then stirred for 1h at room temperature (Solution B). The pre-mixing of the Si and Ti precursors was essential to ensure the incorporation of titanium into the silica nanoparticles. Thereafter, solution B was added dropwise to solution A, resulting in a clear yellowish solution. After 10 min stirring at room temperature, a white precipitate appeared and the solution was further stirred for 2h. The precipitate was subsequently recovered by filtration, washed with distilled H_2O and dried overnight at 75°C. Finally, CTAB was removed by calcination at 550°C for 6h (5°C/min). In the second step, 250 mg of **MSTP** was impregnated with 0.34 ml 40% wt. TPAOH (TPAOH/SiO_2 molar ratio of 0.16) in a crucible and homogenised with a spatula until a homogeneous paste was obtained ($V_{MSTP}/(V_{MSTP} + V_{TPAOH}) = 0.74$). The mixture was then put to rest for 24h. After that time, the solidified paste was crushed manually into small pieces and transferred into a 70 ml teflon-lined stainless steel autoclave containing 20 ml of distilled H_2O in a separate vessel. After 96h SAC at 130°C, the solid was successively washed with distilled water and EtOH so as to facilitate drying without altering the porosity. It was then dried at 75°C overnight and finally calcined at 550°C for 5h (5°C/min).

2.2. Characterization of the materials

The Ti content of the materials was measured by ICP-AES on an ICP 6500 instrument (Thermo Scientific Instrument) after dissolution of the samples by sodium peroxide fusion. XPS experiments were carried out using an SSX 100/206 spectrometer (Surface Science Instruments, USA) with Al-Kα radiation operated at 10 kV and 20 mA. The binding energy scale was calibrated on the Si 2p peak, fixed at 103.5 eV [36]. The quantification of Ti in Ti–O–Si and Ti–O–Ti was based on the decomposition of the $2p_{3/2}$ peak at approximately 460.0 and 458.5 eV, respectively [37,38]. Si was quantified on the basis of the Si 2p peak at 103.5 eV [36]. Powder X-ray diffraction (PXRD) patterns were recorded at room temperature with a D8 ADVANCE Bruker diffractometer equipped with a LYNXEYE XE-T detector, using copper Kα radiation (λ = 1.5418 Å) in a 2θ range of 5–80° (step = 0.02°, time per step = 0.15 s). The X-ray source was operated with a tension of 40 kV and a current of 30 mA. For display, the diffractograms were normalized by the most intense diffraction peak. The DR UV-VIS spectra were recorded on a Shimadzu UV-3600 Plus UV–Vis–NIR Spectrophotometer with a Harrick single-beam Praying Mantis Diffuse Reflectance collection system. The spectra were recorded at room temperature in 20000–50000 cm^{-1} range. A Spectralon® Diffuse Reflectance Standard was used to measure the background spectra. The DR UV-VIS spectra were background corrected, normalized by the most intense absorption band, and the Kulbelka Munk function was used to display the data. Scanning electron microscopy (SEM) images were taken using a JEOL 7600F microscope with a 1–5 kV voltage. Samples were pre-treated with a chromium sputter coating of 15 nm carried out under vacuum with a Sputter Metal 208 HR (Cressington). SEM-FEG pictures were obtained with a Hitachi SU-70. Textural properties were determined from N_2 adsorption/desorption isotherms at -196°C using a Tristar 3000 instrument (Micromeritics, USA). Prior to measurement, the samples were degassed overnight under vacuum at 150°C. The BET specific surface area of **MSTP** was evaluated in the 0.05–0.3 P/P_0 range. For hierarchical zeolites, the external specific surface area – which includes the specific surface area of mesopores – was evaluated by the slope of the line drawn in the linear portion of the t-plot in the 3.5–5 Å thickness range; the micropore volume was given by the intercept. The total pore volume was measured at P/P_0 = 0.98. The pore size distribution was obtained from the adsorption branch using the BJH method.

2.3. Catalytic tests

The catalytic performance was evaluated in water for the epoxidation of allyl alcohol with hydrogen peroxide as the oxidant. The reaction was carried out in a two-necked round-bottomed glass reactor at 45°C, equipped with a magnetic stirrer and a rubber septum. In a typical run, 0.528 g (0.9 M) allyl alcohol (Acros Organics, 99%), 0.037 g (0.05 M) Butan-1-ol (Sigma-Aldrich, ≥ 99.4%) – used as the internal standard – and 50 mg (5 $g.L^{-1}$) catalyst were pre-mixed in 9.152 g of distilled H_2O and stirred for 10 min. To start the reaction, 0.204 g (0.18 M) of 30% (w/w) aqueous H_2O_2 was added and the mixture was allowed to react for 3 h. The product formation was followed by collecting aliquots at regular time intervals and by analysing them

in gas chromatography, using a Varian CP-3800 chromatograph equipped with a FID detector and a capillary column (BR-5, 30 m, 0.32 mm i.d., 1.0 µm film thickness). Prior to injection, water was removed by an extraction step with ethyl acetate (50:50 v/v).

3. Results and discussion

The materials were first analysed by PXRD in order to evaluate the bulk phase crystallinity. The diffractogram of the starting material **MSTP** does not show any peak, confirming the amorphous nature of these Ti–SiO_2 particles. The **TS-1_MAC** catalyst exhibited the crystalline MFI-type structure identical to **TS-1** zeolite (**Figure 1a**). This result demonstrates that the formation of the zeolitic framework in **TS-1_MAC** occurred during the steaming step. Importantly, no TiO_2 anatase – having a signature peak at 2θ = 25° [39,40] – was detected, thereby excluding the presence of large crystalline TiO_2 domains in the materials.

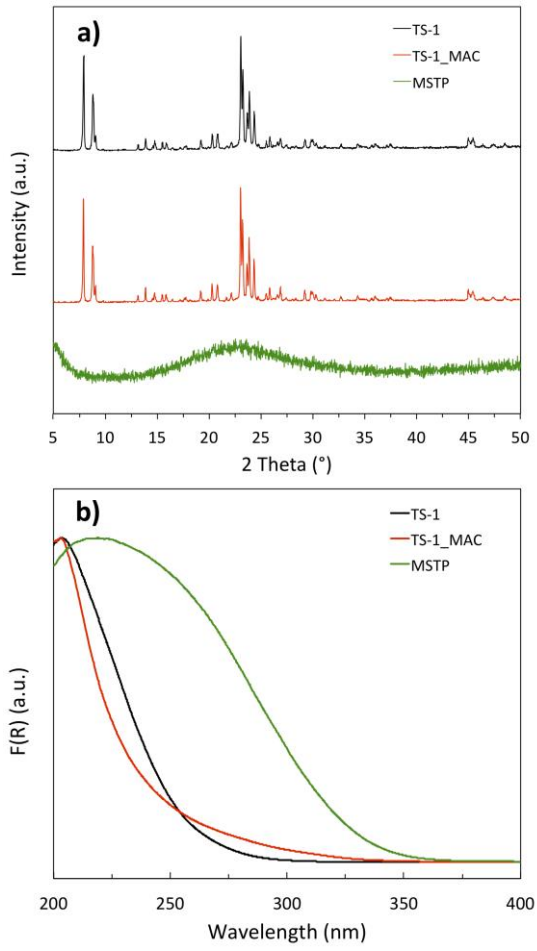

Figure 1. a) Normalized PXRD patterns of the zeolitic catalysts; diffractogram of amorphous **MSTP** is shown for comparison; b) Normalized DR UV-visible spectra of the catalysts (F(R) is the Kubelka-Munk function) and of the starting material **MSTP**.

In order to have deeper insight into the incorporation of titanium in the materials, an elemental analysis was first carried out by ICP-AES and revealed that the experimental Ti content was respectively of 1.6% and 1.7% for **TS-1** and **TS-1_MAC** catalysts (**Table 1**), thus close to the nominal loading. Further investigations by XPS analysis allowed to determine the Ti concentration at the surface as well as the quality of the Ti dispersion (**Table 1** and **Figure S1**, ESI). For both zeolitic catalysts, the surface composition matched closely the bulk content, indicating a homogeneous Ti incorporation throughout the material. On the opposite, the surface Ti content was very low in the starting material **MSTP**, highlighting the fact that Ti is poorly dispersed in the amorphous dry gel, with presumably a gradient of concentration and high Ti content in the bulk of the materials. After applying the SAC procedure, however, a homogeneous zeolitic material is obtained.

Table 1. Percentage of Ti species (mol Ti / (mol Ti + mol Si) × 100 %) in the catalysts (bulk composition, ICP-AES) and at the catalyst surface (from XPS)

	Bulk Ti %[a]	**Surf. Ti %**	**Surf. Ti–O–Si %**	**% Ti–O–Si**[b]
TS-1	1.6 (1.8)	1.3	1.2	90
TS-1_MAC	1.7 (1.8)	1.7	1.0	56
MSTP	–	0.3	–[c]	–

[a] Nominal composition calculated from the precise amounts of precursors actually used in each synthesis is given in brackets. [b] % Ti–O–Si = (Surf. Ti–O–Si % / Surf. Ti %) × 100. [c] The amount of titanium at the surface was too low for this sample to allow a proper decomposition of the Ti 2p peak.

The third column of **Table 1** indicates the fraction of Ti species that are truly dispersed in the silica matrix, forming Ti–O–Si bonds, as determined by the decomposition of the Ti 2p peak [41]. The catalyst prepared by SAC shows a relatively lower Ti dispersion as compared to **TS-1**. As no TiO_2 anatase was detected by PXRD (**Figure 1a**), the fraction that is not well incorporated in the silica matrix is assigned to extra-framework Ti species in 5- and 6-coordination states, possibly in the form of Ti oligomers [42]. This is also suggested by the UV-visible spectrum of the **TS-1_MAC** catalyst (**Figure 1b**), which shows a minor contribution of highly coordinated Ti species in the region between 250 and 300 nm. Nevertheless, the main absorption band for this catalyst is found in the 200–210 nm range – as in **TS-1** – which corresponds to highly dispersed tetrahedral Ti species inside the framework. As a comparison, the XPS spectrum of **MSTP** shows a Ti $2p_{3/2}$ peak at 458.9 eV (see **Figure S1d**, ESI), suggesting a major contribution from Ti–O–Ti bonds present in polymeric Ti oxide species. This result is further supported by the UV-visible spectrum,

which exhibits a much higher contribution of highly coordinated Ti species for **MSTP**, which is a clear indication of the poor dispersion of Ti in this starting material. For this sample, the absorption in the region above 300 nm may not exclude the presence of TiO_2 anatase [43,44]. Yet, these clusters would be too small to be detected by PXRD. In any case, the extra-framework Ti species are converted into framework Ti species by the SAC treatment [13].

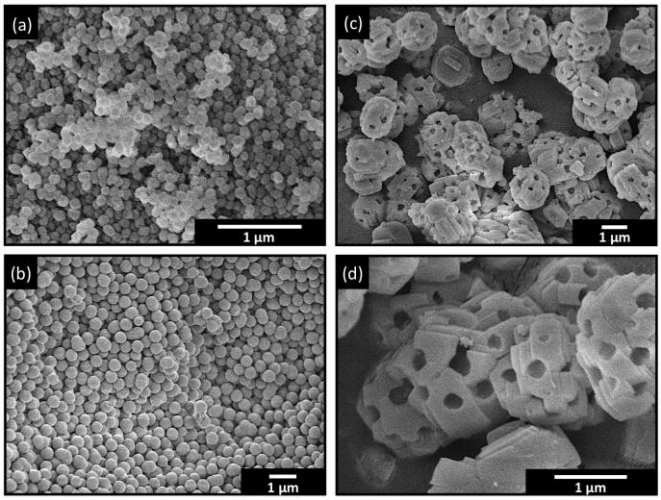

Figure 2. SEM image of a) **TS-1**, b) **MSTP**, and c–d) **TS-1_MAC**.

In SEM, **TS-1_MAC** appeared as holed crystals with size in the 1.5–2 µm range (**Figure 2c–d**), thus ~ 15 times larger than the typical nano-sized crystals of **TS-1** which show dimensions between 100 and 150 nm (**Figure 2a**) [35]. **TS-1_MAC** crystals are smaller than the Ti-free silicalite-1 crystals prepared by Machoke et al. (*ca.* 4 µm) [33], which suggests a lower rate of crystallization in the presence of titanium [35]. This assumption is further supported by the fact that the crystallization did not occur when performing the SAC at 110°C, as indicated for silicalite-1 [33]. In the present case, the crystallisation step had to be carried out at 130°C to obtain the crystalline TS-1. Each embedded macropore in **TS-1_MAC** has a pore opening between 200 and 300 nm. These macropores are a reminiscence of the individual **MSTP** particles (see **Figure 2b**) which have an average diameter of *ca.* 450 nm and serve both as a precursor for the TS-1 crystallization and as a hard template.

From the above, the mechanism of formation of **TS-1_MAC** crystals can be schematized as represented in **Scheme 1**. Each crystal is formed by a hard templating route, in which the embedded macropores result from the dissolution-recrystallization of the amorphous **MSTP** particles upon steaming in the presence of the structure directing agent [33]. During this key step, the poorly dispersed Ti species in the amorphous precursor particles are incorporated in the zeolitic framework in a 4-coordination mode. The crystals then grow *via* the oriented attachment of tiny crystallites, following the mechanism proposed by Song *et al.* [29].

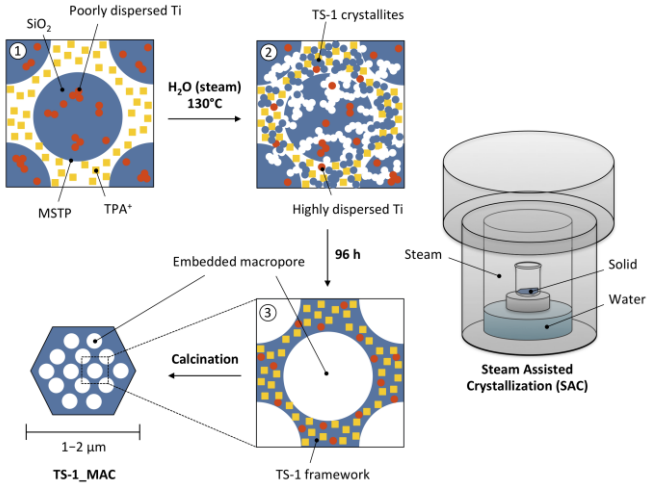

Scheme 1. Proposed mechanism of formation of **TS-1_MAC**. In step 1, the **MSTP** particles are surrounded by the zeolite structure directing agent. In step (2), the dissolution-recrystallization proceeds in the presence of the SDA upon steaming to form tiny TS-1 crystallites which aggregate around the precursor particles to form bigger crystals. In step (3), the hierarchical zeolite framework is fully crystallized and displays embedded macropores.

In N_2 physisorption, the isotherms of the **MSTP** solid revealed the presence of supermicropores formed upon templating with CTAB. Yet, no micropores were found on the t-plot. After the SAC treatment, **TS-1_MAC** expectedly showed a Type I isotherm characteristic of microporous solids, and very close to the **TS-1** sample (**Figure 3**). The micropore volume V_μ is similar in both catalysts (**Table 2**). Although the macropores of **TS-1_MAC** fall off the measurment range of the N_2 physisorption technique, the forced closure of the isotherm upon desorption at P/P_0 of 0.4–0.5 due to the tensile stress effect [45] suggests also the presence of mesopores smaller than 3.8 nm in the pore walls of the material, as reported in the literature [33,46] (see also inset of **Figure 3**). The large N_2 uptake at high P/P_0 in this sample is assigned to interparticular voids between the crystals (~ 40–50 nm). The external surface area of **TS-1** nanosized crystals was of 130 $m^2.g^{-1}$. Importantly, despite the much larger crystal size of **TS-1_MAC**, the external surface area reached 150 $m^2.g^{-1}$ (**Table 2**), thanks to the surface area generated by the additional porosity.

Table 2. Textural properties of the catalysts

	S_{ext} ($m^2.g^{-1}$)[a]	V_μ ($cm^3.g^{-1}$)[a]	V_p ($cm^3.g^{-1}$)[b]
TS-1	130	0.15	0.28
TS-1_MAC	150	0.14	0.23
MSTP	610[c]	0	0.40

[a]Calculated from the t-plot. [b]Measured at P/P_0 = 0.98. [c]For this sample, the external surface area is evaluated by the BET method.

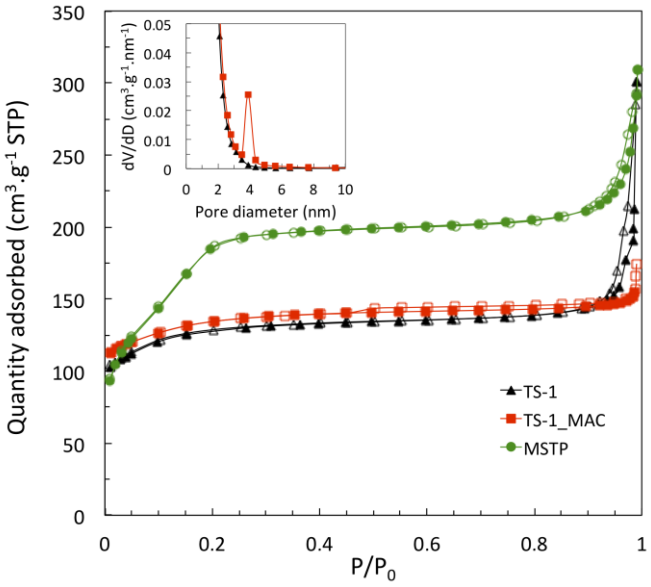

Figure 3. N_2 adsorption-desorption isotherms of the materials. Desorption PSDs of **TS-1** and **TS-1_MAC** are shown in inset.

The catalytic performance of **TS-1_MAC** was evaluated for the epoxidation of allyl alcohol to glycidol in water with H_2O_2 as the oxidizing agent. From the kinetic curves presented in **Figure 4** – showing the glycidol production over time – almost no activity was observed when testing the amorphous **MSTP** starting material. Indeed, it is well known that amorphous Ti–SiO_2 catalysts are sensitive to the presence of H_2O molecules [47], leading to strong deactivation issues in the presence of large amounts of water [48]. Besides, XPS and UV-visible spectroscopy showed that Ti was poorly dispersed in the **MSTP** sample (*vide supra*). On the opposite, **TS-1_MAC** was highly active as it showed similar performance as the benchmark **TS-1**. Thus, starting from an inactive Ti-SiO_2 material, an active epoxidation catalyst is obtained using SAC. The high activity of this material can be ascribed to the successful formation of the MFI crystal structure upon steaming (see **Figure 1**). Indeed, the incorporation of single site Ti in the crystalline framework during the dissolution-recrystallization step accounts for the formation of the active sites, and the MFI structure is known to confer an intrinsic resistance towards deactivation in water.

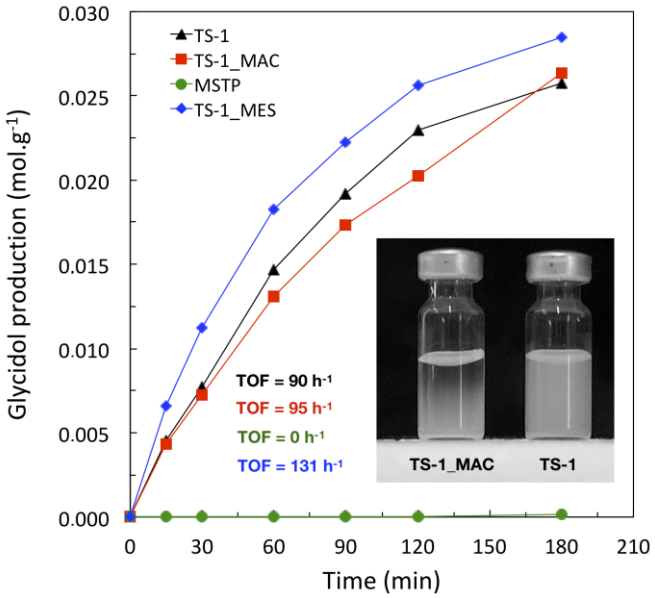

Figure 4. Kinetic data for the conversion of allyl alcohol into glycidol in H_2O using aqueous solution of hydrogen peroxide as oxidizing agent. The initial turnover frequency (TOF) was approximated by the glycidol production after 15 min reaction time and normalized by the amount of active Ti (see "Surf. Ti–O–Si %" in **Table 1**). No other products were detected. Experimental conditions: T = 45°C, [Allyl alcohol] = 0.9 $mol.l^{-1}$, [H_2O_2] = 0.18 $mol.l^{-1}$. In inset is shown a picture illustrating the fact that the **TS-1_MAC** sample settles faster than **TS-1** in water. The picture was taken 2h after sonicating the catalyst suspension (20 $g.l^{-1}$) for 30 min.

Both **TS-1** and **TS-1_MAC** exhibit comparable performance, not only in terms of glycidol production and full selectivity towards the epoxide [49], but also as regard to their turnover frequency (TOF). Yet, increasing the particle size gives a competitive advantage by reducing the energy cost for separation by facilitating the catalyst recovery by centrifugation or filtration. For example, the sedimentation behaviour was qualitatively assessed for both **TS-1_MAC** and **TS-1** and we showed that the former could be separated much faster (see inset of **Figure 4**). Zuo *et al.* have shown, however, that the turnover frequency decreases when increasing the crystal size of non-hierarchical TS-1, because the external surface areas was lowered (85 and 145 $m^2.g^{-1}$ for crystal size of 1200 and 200 nm, respectively) [50]. In our system, the key factor is that the additional porosity of **TS-1_MAC** allows to overcome this limitation. While switching from ~100 nm **TS-1** particles to ~1500 nm crystals of **TS-1_MAC**, a high external surface area is maintained (S_{ext} = 130 $m^2.g^{-1}$ and 150 $m^2.g^{-1}$ respectively).

The beneficial effect of the introduction of a hierarchical porosity in TS-1 on the catalytic performance was previously reported for micro-/mesoporous TS-1. In order to compare **TS-1_MAC** to

such type of catalyst, a micro-/mesoporous TS-1 – denoted **TS-1_MES** – was synthesized with the same structure and composition according to a typical procedure from the literature (see ESI for detailed synthesis procedure and full characterization) [31]. We confirm the validity of such approach, as this catalyst showed slightly higher performance than **TS-1** and **TS-1_MAC** (**Figure 4**). This results from the increased pore volume (0.41 $cm^3.g^{-1}$) and external surface area (180 $m^2.g^{-1}$) owing to the additional presence of mesopores. It should be noted however that this synthesis involves the use of a sacrificial soft templating agent, whereas the SAC method does not require any additional template. Besides, the amount of TPAOH used here remains quite low (TPAOH/Si ≈ 0.16) compared to other hierarchical TS-1 (TPAOH/Si = 0.21 for **TS-1_MES** [31]) and conventional TS-1 (TPAOH/Si = 0.41 [35]). These two characteristics may contribute to reduce the cost of fabrication of the catalyst, which is of outmost importance for the industrial use of TS-1 based catalysts [51].

4. Conclusion

Herein, we show that combining titanium and silicon precursors in the preparation of amorphous Ti–SiO_2 nanoparticles followed by steam assisted crystallization in the presence of TPAOH allowed obtaining a micro-/macroporous titanosilicate zeolite with the MFI-type structure. The crystals of this new macro-microporous TS-1 catalyst are about 15 times larger than the nanosized TS-1 benchmark. Yet their external surface area remained relatively high, owing to the presence of the macropores. This catalyst performed as well as the nanosized TS-1 zeolite in the epoxidation of allyl alcohol in water. Notably, the larger crystal size ensures an easier recovery of the material.

Acknowledgements

Authors acknowledge the 'Communauté française de Belgique' for the financial support through the ARC programme (15/20-069). F. Devred is acknowledged for the technical and logistical support. V. Smeets is thankful to F.R.S.–F.N.R.S for his FRIA PhD grant. F.R.S.–F.N.R.S is also thanked for the acquisition of the (i) DR UV-visible equipment used (project CDRJ.0156.18, supervisor E. M. Gaigneaux) and of the (ii) X-ray diffraction equipment used (project EQP U.N006.16F, supervisor E. M. Gaigneaux).

References

[1] M. Taramasso, G. Perego, B. Notari, Preparation of porous crystalline synthetic material comprised of silicon and titanium oxides, US4410501A, 1983. https://patents.google.com/patent/US4410501A/en (accessed August 21, 2018).

[2] M.G. Clerici, P. Ingallina, Epoxidation of Lower Olefins with Hydrogen Peroxide and Titanium Silicalite, Journal of Catalysis. 140 (1993) 71–83. doi:10.1006/jcat.1993.1069.

[3] J. Přech, Catalytic performance of advanced titanosilicate selective oxidation catalysts – a review, Catalysis Reviews. 60 (2018) 71–131. doi:10.1080/01614940.2017.1389111.

[4] M. Hartmann, A.G. Machoke, W. Schwieger, Catalytic test reactions for the evaluation of hierarchical zeolites, Chem. Soc. Rev. 45 (2016) 3313–3330. doi:10.1039/C5CS00935A.

[5] V. Smeets, C. Boissière, C. Sanchez, E.M. Gaigneaux, E. Peeters, B.F. Sels, M. Dusselier, D.P. Debecker, Aerosol Route to TiO2–SiO2 Catalysts with Tailored Pore Architecture and High Epoxidation Activity, Chem. Mater. 31 (2019) 1610–1619. doi:10.1021/acs.chemmater.8b04843.

[6] V. Smeets, L. van den Biggelaar, T. Barakat, E.M. Gaigneaux, D.P. Debecker, Macrocellular Titanosilicate Monoliths as Highly Efficient Structured Olefin Epoxidation Catalysts, ChemCatChem. 11 (2019) 1593–1597. doi:10.1002/cctc.201900028.

[7] S. Li, J. Li, M. Dong, S. Fan, T. Zhao, J. Wang, W. Fan, Strategies to control zeolite particle morphology, Chem. Soc. Rev. (2019). doi:10.1039/C8CS00774H.

[8] K. Na, C. Jo, J. Kim, W.-S. Ahn, R. Ryoo, MFI Titanosilicate Nanosheets with Single-Unit-Cell Thickness as an Oxidation Catalyst Using Peroxides, ACS Catal. 1 (2011) 901–907. doi:10.1021/cs2002143.

[9] J. Přech, P. Eliášová, D. Aldhayan, M. Kubů, Epoxidation of bulky organic molecules over pillared titanosilicates, Catalysis Today. 243 (2015) 134–140. doi:10.1016/j.cattod.2014.07.002.

[10] M.-H. Zhu, L. Li, L. Chen, Y.-X. Liao, W.-J. Ding, Z.-J. Feng, Z. Wan, N. Hu, X.-S. Chen, H. Kita, Preparation of TS-1 zeolite membrane from dilute precursor synthesis solution, Microporous and Mesoporous Materials. 273 (2019) 212–218. doi:10.1016/j.micromeso.2018.07.017.

[11] Z. Han, Y. Shen, X. Qin, F. Wang, X. Zhang, G. Wang, H. Li, Synthesis of Hierarchical Titanium-Rich Titanium Silicalite-1 Zeolites and the Highly Efficient Catalytic Performance for Hydroxylation of Phenol, ChemistrySelect. 4 (2019) 1618–1626. doi:10.1002/slct.201803864.

[12] G. Xiong, D. Hu, Z. Guo, Q. Meng, L. Liu, An efficient Titanium silicalite-1 catalyst for propylene epoxidation synthesized by a combination of aerosol-assisted hydrothermal synthesis and recrystallization, Microporous and Mesoporous Materials. 268 (2018) 93–99. doi:10.1016/j.micromeso.2018.04.015.

[13] Y. Jiao, A.-L. Adedigba, Q. He, P. Miedziak, G. Brett, N.F. Dummer, M. Perdjon, J. Liu, G.J. Hutchings, Inter-connected and open pore hierarchical TS-1 with

controlled framework titanium for catalytic cyclohexene epoxidation, Catal. Sci. Technol. 8 (2018) 2211–2217. doi:10.1039/C7CY02571H.

[14] M.B. Yue, M.N. Sun, F. Xie, D.D. Ren, Dry-gel synthesis of hierarchical TS-1 zeolite by using P123 and polyurethane foam as template, Microporous and Mesoporous Materials. 183 (2014) 177–184. doi:10.1016/j.micromeso.2013.09.029.

[15] Y. Zuo, T. Zhang, M. Liu, Y. Ji, C. Song, X. Guo, Mesoporous/Microporous Titanium Silicalite with Controllable Pore Diameter for Cyclohexene Epoxidation, Ind. Eng. Chem. Res. 57 (2018) 512–520. doi:10.1021/acs.iecr.7b03719.

[16] S.-K. Kim, B.M. Reddy, S.-E. Park, High-Performance Microwave Synthesized Mesoporous TS-1 Zeolite for Catalytic Oxidation of Cyclic Olefins, Ind. Eng. Chem. Res. 57 (2018) 3567–3574. doi:10.1021/acs.iecr.7b04556.

[17] H. Xin, J. Zhao, S. Xu, J. Li, W. Zhang, X. Guo, E.J.M. Hensen, Q. Yang, C. Li, Enhanced Catalytic Oxidation by Hierarchically Structured TS-1 Zeolite, J. Phys. Chem. C. 114 (2010) 6553–6559. doi:10.1021/jp912112h.

[18] S. Du, X. Chen, Q. Sun, N. Wang, M. Jia, V. Valtchev, J. Yu, A non-chemically selective top-down approach towards the preparation of hierarchical TS-1 zeolites with improved oxidative desulfurization catalytic performance, Chem. Commun. 52 (2016) 3580–3583. doi:10.1039/C5CC10232D.

[19] L.-H. Chen, X.-Y. Li, G. Tian, Y. Li, J.C. Rooke, G.-S. Zhu, S.-L. Qiu, X.-Y. Yang, B.-L. Su, Highly Stable and Reusable Multimodal Zeolite TS-1 Based Catalysts with Hierarchically Interconnected Three-Level Micro–Meso–Macroporous Structure, Angew. Chem. Int. Ed. 50 (2011) 11156–11161. doi:10.1002/anie.201105678.

[20] W. Cheng, Y. Jiang, X. Xu, Y. Wang, K. Lin, P.P. Pescarmona, Easily recoverable titanosilicate zeolite beads with hierarchical porosity: Preparation and application as oxidation catalysts, Journal of Catalysis. 333 (2016) 139–148. doi:10.1016/j.jcat.2015.09.017.

[21] J. Lin, F. Xin, L. Yang, Z. Zhuang, Synthesis, characterization of hierarchical TS-1 and its catalytic performance for cyclohexanone ammoximation, Catalysis Communications. 45 (2014) 104–108. doi:10.1016/j.catcom.2013.11.005.

[22] Y. Wang, M. Lin, A. Tuel, Hollow TS-1 crystals formed via a dissolution–recrystallization process, Microporous and Mesoporous Materials. 102 (2007) 80–85. doi:10.1016/j.micromeso.2006.12.019.

[23] C. Pagis, A.R. Morgado Prates, D. Farrusseng, N. Bats, A. Tuel, Hollow Zeolite Structures: An Overview of Synthesis Methods, Chem. Mater. 28 (2016) 5205–5223. doi:10.1021/acs.chemmater.6b02172.

[24] Z. Guo, G. Xiong, L. Liu, P. Li, L. Hao, Y. Cao, F. Tian, Aerosol-assisted synthesis of hierarchical porous titanosilicate molecular sieve as catalysts for cyclohexene epoxidation, J Porous Mater. 23 (2016) 407–413. doi:10.1007/s10934-015-0094-7.

[25] L. Lakiss, M. Rivallan, J.-M. Goupil, J. El Fallah, S. Mintova, Self-assembled titanosilicate TS-1 nanocrystals in hierarchical structures, Catalysis Today. 168 (2011) 112–117. doi:10.1016/j.cattod.2010.12.045.

[26] W.J. Kim, T.J. Kim, W.S. Ahn, Y.J. Lee, K.B. Yoon, Synthesis, Characterization and Catalytic Properties of TS-1 Monoliths, Catalysis Letters. 91 (2003) 123–127. doi:10.1023/B:CATL.0000006327.29961.26.

[27] H. Liu, G. Lu, Y. Guo, Y. Guo, J. Wang, Deactivation and regeneration of TS-1/diatomite catalyst for hydroxylation of phenol in fixed-bed reactor, Chemical Engineering Journal. 108 (2005) 187–192. doi:10.1016/j.cej.2005.01.011.

[28] K. Möller, B. Yilmaz, R.M. Jacubinas, U. Müller, T. Bein, One-Step Synthesis of Hierarchical Zeolite Beta via Network Formation of Uniform Nanocrystals, J. Am. Chem. Soc. 133 (2011) 5284–5295. doi:10.1021/ja108698s.

[29] W. Song, Z. Liu, L. Liu, A.L. Skov, N. Song, G. Xiong, K. Zhu, X. Zhou, A solvent evaporation route towards fabrication of hierarchically porous ZSM-11 with highly accessible mesopores, RSC Adv. 5 (2015) 31195–31204. doi:10.1039/C5RA02493E.

[30] Y. Zhang, K. Zhu, X. Zhou, W. Yuan, Synthesis of hierarchically porous ZSM-5 zeolites by steam-assisted crystallization of dry gels silanized with short-chain organosilanes, New J. Chem. 38 (2014) 5808–5816. doi:10.1039/C4NJ00811A.

[31] Z. Kong, B. Yue, W. Deng, K. Zhu, M. Yan, Y. Peng, H. He, Direct synthesis of hierarchically porous TS-1 through a solvent-evaporation route and its application as an oxidation catalyst, Appl. Organometal. Chem. 28 (2014) 239–243. doi:10.1002/aoc.3115.

[32] Q. Du, Y. Guo, P. Wu, H. Liu, Y. Chen, Facile synthesis of hierarchical TS-1 zeolite without using mesopore templates and its application in deep oxidative desulfurization, Microporous and Mesoporous Materials. 275 (2019) 61–68. doi:10.1016/j.micromeso.2018.08.018.

[33] A.G. Machoke, A.M. Beltrán, A. Inayat, B. Winter, T. Weissenberger, N. Kruse, R. Güttel, E. Spiecker, W. Schwieger, Micro/macroporous system: MFI-type zeolite crystals with embedded macropores, Adv. Mater. Weinheim. 27 (2015) 1066–1070. doi:10.1002/adma.201404493.

[34] T. Weissenberger, B. Reiprich, A.G.F. Machoke, K. Klühspies, J. Bauer, R. Dotzel, J.L. Casci, W. Schwieger, Hierarchical MFI type zeolites with intracrystalline macropores: the effect of the macropore size on the deactivation behaviour in the MTO reaction, Catal. Sci. Technol. 9 (2019) 3259–3269. doi:10.1039/C9CY00368A.

[35] A. Thangaraj, M.J. Eapen, S. Sivasanker, P. Ratnasamy, Studies on the synthesis of titanium silicalite, TS-1, Zeolites. 12 (1992) 943–950. doi:10.1016/0144-2449(92)90159-M.

[36] M. Jacquemin, M.J. Genet, E.M. Gaigneaux, D.P. Debecker, Calibration of the X-Ray Photoelectron Spectroscopy Binding Energy Scale for the

Characterization of Heterogeneous Catalysts: Is Everything Really under Control?, ChemPhysChem. 14 (2013) 3618–3626. doi:10.1002/cphc.201300411.

[37] B.M. Reddy, B. Chowdhury, P.G. Smirniotis, An XPS study of the dispersion of MoO3 on TiO2–ZrO2, TiO2–SiO2, TiO2–Al2O3, SiO2–ZrO2, and SiO2–TiO2–ZrO2 mixed oxides, Applied Catalysis A: General. 211 (2001) 19–30. doi:10.1016/S0926-860X(00)00834-6.

[38] B. Erdem, R.A. Hunsicker, G.W. Simmons, E.D. Sudol, V.L. Dimonie, M.S. El-Aasser, XPS and FTIR Surface Characterization of TiO2 Particles Used in Polymer Encapsulation, Langmuir. 17 (2001) 2664–2669. doi:10.1021/la0015213.

[39] B.S. Shirke, P.V. Korake, P.P. Hankare, S.R. Bamane, K.M. Garadkar, Synthesis and characterization of pure anatase TiO2 nanoparticles, J Mater Sci: Mater Electron. 22 (2011) 821–824. doi:10.1007/s10854-010-0218-4.

[40] A. Kim, C. Sanchez, G. Patriarche, O. Ersen, S. Moldovan, A. Wisnet, C. Sassoye, D. P. Debecker, Selective CO 2 methanation on Ru/TiO 2 catalysts: unravelling the decisive role of the TiO 2 support crystal structure, Catalysis Science & Technology. 6 (2016) 8117–8128. doi:10.1039/C6CY01677D.

[41] L.E. Manangon-Perugachi, A. Vivian, P. Eloy, D.P. Debecker, C. Aprile, E.M. Gaigneaux, Hydrophobic titania-silica mixed oxides for the catalytic epoxidation of cyclooctene, Catalysis Today. (2019). doi:10.1016/j.cattod.2019.05.020.

[42] A.M. Cojocariu, P.H. Mutin, E. Dumitriu, F. Fajula, A. Vioux, V. Hulea, Mild oxidation of bulky organic compounds with hydrogen peroxide over mesoporous TiO2-SiO2 xerogels prepared by non-hydrolytic sol–gel, Applied Catalysis B: Environmental. 97 (2010) 407–413. doi:10.1016/j.apcatb.2010.04.027.

[43] G. Berlier, V. Crocellà, M. Signorile, E. Borfecchia, F. Bonino, S. Bordiga, Characterization of Metal Centers in Zeolites for Partial Oxidation Reactions, in: J. Pérez Pariente, M. Sánchez-Sánchez (Eds.), Structure and Reactivity of Metals in Zeolite Materials, Springer International Publishing, Cham, 2018: pp. 91–154. doi:10.1007/430_2018_24.

[44] K. Madhusudan Reddy, S.V. Manorama, A. Ramachandra Reddy, Bandgap studies on anatase titanium dioxide nanoparticles, Materials Chemistry and Physics. 78 (2003) 239–245. doi:10.1016/S0254-0584(02)00343-7.

[45] J.C. Groen, L.A.A. Peffer, J. Pérez-Ramírez, Pore size determination in modified micro- and mesoporous materials. Pitfalls and limitations in gas adsorption data analysis, Microporous and Mesoporous Materials. 60 (2003) 1–17. doi:10.1016/S1387-1811(03)00339-1.

[46] J.P. Thielemann, F. Girgsdies, R. Schlögl, C. Hess, Pore structure and surface area of silica SBA-15: influence of washing and scale-up, Beilstein Journal of Nanotechnology. 2 (2011) 110–118. doi:10.3762/bjnano.2.13.

[47] G. Deo, A.M. Turek, I.E. Wachs, D.R.C. Huybrechts, P.A. Jacobs, Characterization of titania silicalites, Zeolites. 13 (1993) 365–373. doi:10.1016/0144-2449(93)90151-R.

[48] V. Smeets, L. Ben Mustapha, J. Schnee, E.M. Gaigneaux, D.P. Debecker, Mesoporous SiO2-TiO2 epoxidation catalysts: Tuning surface polarity to improve performance in the presence of water, Molecular Catalysis. 452 (2018) 123–128. doi:10.1016/j.mcat.2018.04.011.

[49] M.G. Clerici, The activity of titanium silicalite-1 (TS-1): Some considerations on its origin, Kinet Catal. 56 (2015) 450–455. doi:10.1134/S0023158415040059.

[50] Y. Zuo, M. Liu, T. Zhang, C. Meng, X. Guo, C. Song, Enhanced Catalytic Performance of Titanium Silicalite-1 in Tuning the Crystal Size in the Range 1200–200 nm in a Tetrapropylammonium Bromide System, ChemCatChem. 7 (2015) 2660–2668. doi:10.1002/cctc.201500440.

[51] G. Ming-Xing, G. Hong-Chen, W. Xiang-Sheng, G. Wei-Min, Gas Phase Epoxidation of Propylene with O2 Induced by Alternating Electric Field, Chinese Journal of Chemistry. 23 (2005) 471–473. doi:10.1002/cjoc.200590471.